Industrial Tomographic Gamma Scan for Demister Evaluation

Marcio I. Haraguchi[*1], *HaeYong Kim*[2]

1 - Tricom Tecnologia, Av. Conselheiro Rodrigues Alves, 58, Piquete, SP, Brazil. E-mail: marcio@tricomtecnologia.com.br.

2 - Universidade de São Paulo, Escola Politécnica, Av. Prof. Luciano Gualberto, tr. 3, 158, São Paulo, SP, Brazil. E-mail: hae.kim@usp.br.

ABSTRACT

The industrial tomographic 2-D gamma scan is an innovative non-destructive nuclear test designed to troubleshoot problems with process equipment, such as distillation columns and reactors.Due to physical restrictions, normally the gamma ray source and detector can only be positioned laterally to the equipment. The 2-D gamma scan is able to reconstruct the interior of the equipment even under this restriction, generatingrectangular 2-D axial densityprofiles of equipment.To obtain clear reconstructions, it is necessary to collimate the detector, discarding the divergent incoming rays. It is not possible to use physical collimation in an industrial environment, as it is impossible to point the detector precisely in the direction of the gamma-ray emitter. In this article, we describe a technique we call “electronic collimation for gamma scan” that allows obtaining collimated data without physical collimation. We use 2-D gamma scan toevaluate a huge dilution steam drum in a large petrochemical plantto investigate possible problems with three demister pads. The low density of the demisters when compared to the vessel and surroundings makes it difficult to generate a reconstructed image where demisters are clearly visible.We describe how we overcome these difficulties using information known a priori about the equipment. We also ran simulations to show the superiority of 2-D gamma scan over conventional scan. These simulations also showed that, if there were defects in the demisters, we would observe them in the reconstructed images. We conclude that electronic collimation and prior informationare essential for evaluating properly equipment with challenging layouts and low density parts.

KEYWORDS

Tomographic gamma scan, gamma scan, industrial computed tomography, demister, process equipment, electronic collimation, algebraic reconstruction technique, total variation minimization, compressive sensing.

1. Introduction

Gamma ray scanning is a nuclear inspection technique widely used to diagnose and solve production issues in industrial equipment. In this technique, a radiation source and detector move along the equipment's longitudinal axis, and the intensity readings generate the equipment's 1-D longitudinal density profile [1-5].

On the other hand, industrial gamma ray computed tomography (CT) uses gamma radiation and tomographic reconstruction to produce the density profile of the interior of an industrial equipment [6,7]. Many industrial CT requires that the analyzed equipment must be placed inside a gantry that rotates to automate the data acquisition process [8,9]. Using CT technique with gantry, huge industrial equipment, such as petrochemical distillation column, cannot be scanned, because it is impossible to place a huge apparatus inside the gantry. However, it is possible to place source and detector of gamma rays in determined locations without using gantry [9,10,11]. This way, even enormous industrial equipment can be scanned by CT. Industrial CT usually produces a circular 2-D density profile of the equipment's cross section.

Haraguchi et al. have proposed industrial tomographic 2-D gamma scan, an improvement over the conventional 1-D gamma scan, developed to solve problems of industrial process equipment like distillation columns, reactors, pipings and other process vessels [12]. This system uses a special irradiation geometry, with the gamma ray source and detector positioned laterally to the equipment.Industrial equipment usually has its length (or height), much greater than its diameter and so there is no other practical way to position the instruments. The radiation beams cross the section under analysis in different angles, to produce a rectangular 2-D profile of axial densities of the evaluated section (Figure 1). As far as we know, this is the first applied industrial tomographic system that produces reconstruction in a rectangular domain under these constraints.

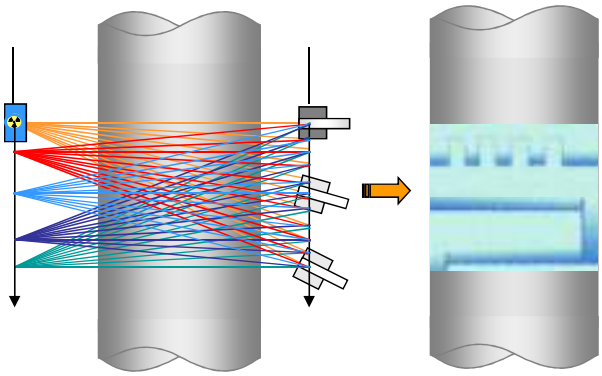

Figure 1. The image on the left shows the positions of the source and detector of gamma ray used in the tomographic 2-D gamma scan. The image on the right shows the internal parts of the equipment to be reconstructed by the 2-D scan.

Collimation is the process of emitting/collecting gamma rays only to/from a given direction. Gamma ray tomography for small objects generally uses mechanical collimation in the detector that attenuates divergent incoming radiation and consequently allows obtaining sharp reconstructed images. On the other hand, 1-D gamma scan usually does not use any mechanical collimation in the detector because it is only interested in obtaining a relative density profile. In 2-D gamma scan, we cannot use mechanical collimation because it is impossible to precisely point the collimated detector at the source. However, if we do not collimate, we would obtain blurred reconstructed images, as the detector would capture gamma rays from a wide angle. This paper describes a technique we named “electronic collimation for gamma scan” that allows obtaining sharp reconstructed images even without any mechanical collimation.

We appliedelectronic collimation toscan a real industrial equipment. A large petrochemical plant in southwestern Brazil wanted to investigate if there is any problem in a dilution steam drum with three demisters. One of the difficulties in inspecting a demister with gamma rays is its low density. Linear absorption coefficient for Co-60 on steel is 0.42 cm^{-1} and on water is 0.063 cm^{-1}. Meanwhile, the estimated attenuation factor of demister is only 0.0105 cm^{-1}, that is, 40 times less dense than steel and 6 times less dense than water. It is difficult to visualize such a light material, especially when it is enclosed within a vessel with dense steel walls. This

paperdescribes how we overcome this difficulty by feeding 2D tomographic gamma scanwith prior knowledge about the digitized equipment, together with artificial irradiation data.

We also made simulations to certify that, if there were any mechanical defects in the demisters, we would see them in the reconstructed images. These simulations also allowed us to assess the superiority of the 2-D gamma scan over the conventional 1-D method.

This paper is organized as follows. In Section 2, we describe conventional gamma ray techniques to evaluate demister pads, that is, 1-D scan and computed tomography, using real industrial examples. In Section 3, we describe the tomographic reconstruction problem and algorithms, as well asthe“electronic collimation for gamma scan”. In Section 4, we describe how we evaluated the long vessel with three demisters pads using tomographic 2-D scan. In Section 5, we present simulations, and quantitative and qualitative comparisonsbetween 1-D and2-D scans. Finally, we present our conclusions in Section 6.

2. Conventional Techniques to Evaluate Demister Pads

In this Section, we use real industrial examples to illustrate two conventional gamma ray techniques to inspect demister pads: gamma scan and computed tomography.

In process industries, such as refineries and petrochemical plants, whenever liquid and gases come into contact, small particles of liquids can be entrained by the flow of steam. These liquids can cause inefficiencies or problems downstream [13]. Some special devices, called demisters, are placed in the vapor path, obstructing the free movement of liquid droplets and forcing them to coalesce into larger drops that cannot be entrained by the flow of vapor (Figure 2).

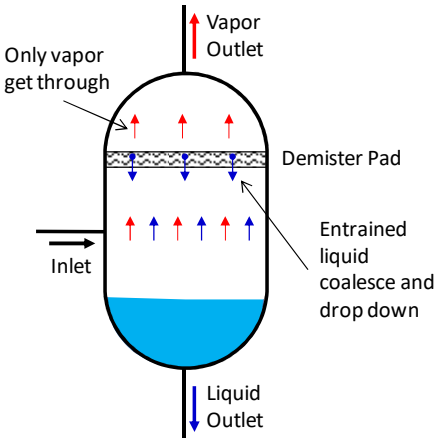

Figure 2. Principle of operation of the demister.

As any process equipment, demisters are susceptible to failure, most often by fouling or mechanical damage due to their light structure. Since the process equipment where these demisters are mounted consists of steel containers with little or no visual indication of its internal parts, non-destructive testing (NDT) such as gamma scanning and industrial tomography should be used to inspect its interior.

2.1. Conventional Gamma Scan

When NDT is performed, its results may not be accurate or may not clearly indicate the problem. For example, Figure 3 shows part of conventional 1-D gamma-ray scan of a distillation column with a demister at the top. Although the scans diagnosed that most of the demister appears to be in place, no further information could be obtained from the plot.

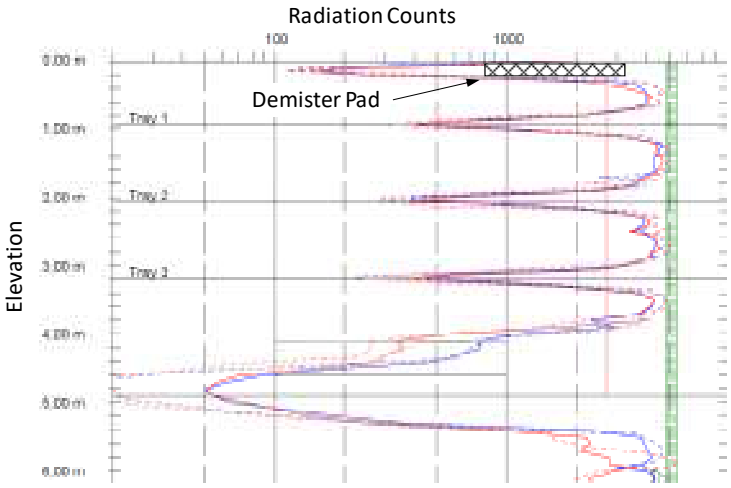

Figure 3. The result of a conventional gamma scan of a demister pad.

2.2. Industrial Computed Tomography

Industrial Computed Tomography (CT) has become available at industrial plants approximately 20 years ago [14]. This technology is useful to improve the results of traditional gamma scan, offering the possibility to further evaluate the density distribution in process equipment such as packed columns, reactors and demisters [15,16]. Figure 4 depicts a knockout drum evaluated with CT at the elevation of the demister. This plant has been suffering deleterious effects from liquids transported downstream, so a mechanical damage to the demister was suspected. The CT results showed that, instead of a mechanical damage, the central area of the demister was denser than the peripheral area, indicating that the mesh was saturated with polymer fouling that prevented it from operating properly and causing liquid entrainment [17].

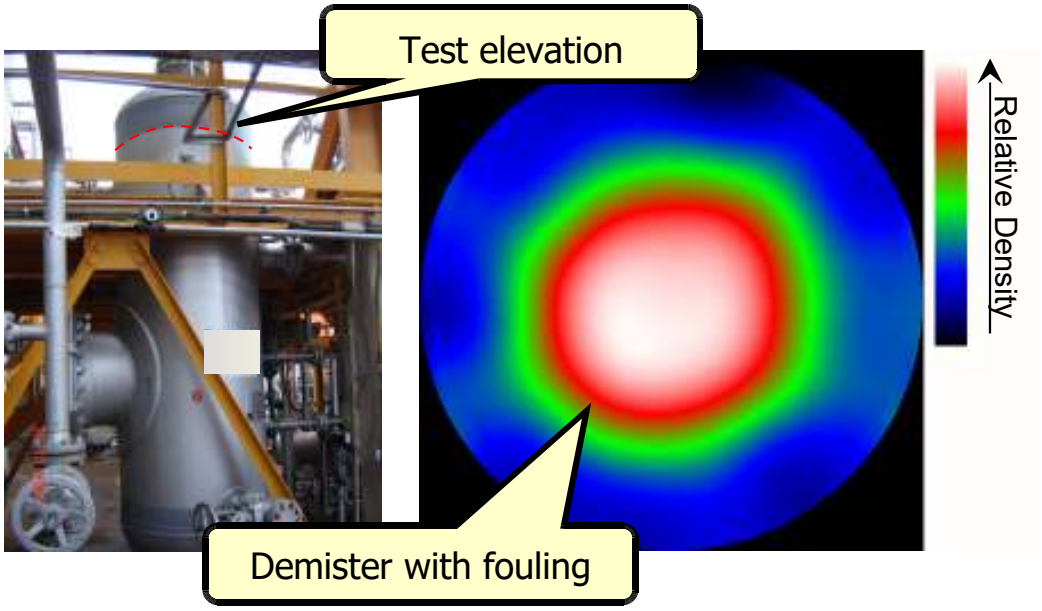

Figure 4. Industrial tomography of a demister pad.

When the equipment was shut down for maintenance, an inspection of the demister confirmed the CT results. Figure 5 depicts the fouled appearance of the demister just after opening the vessel.In this project, we have already used a preliminary concept of “electronic collimation for gamma scanning”, which we will describe in detail below.

Figure 5. Inspection of the demister pad confirmed that it was saturated with polymer fouling.

3. Tomographic Reconstruction and Electronic Collimation for Gamma Scan

This section describes the gamma ray tomographic reconstruction problem and algorithms. It also presents a technique we named "electronic collimation for gamma scan", essential for obtaining sharp reconstructions from 2-D gamma scan.

3.1. Tomographic reconstruction

3.1.1. The problem

When gamma ray passes through material, it is attenuated according to the Beer-Lambert's law:

$$I = I_E \exp\left[-\int_r \mu(x,y)dr\right] \quad (1)$$

where I is the intensity of detected radiation, I_E is the intensity of emitted radiation, $\mu(x, y)$ is the linear attenuation coefficient at point (x, y) and r is the gamma ray path. The emitted intensity I_E is unknown. In order to compute the integral $\int_r \mu(x,y)dr$without knowing I_E, we use the "calibration intensity"I_0 measured by the detector, separating the radiation source and the detector by a known distance of d_0 in a medium with irrelevant attenuation, that is, vacuum or air. Using the calibration intensity I_0,the calibration distance d_0 and the law of squares, we can estimate the radiation intensity I_1that would be detected ifthe radiation source and the detector were separated by distance d_1 in vacuum or air:

$$I_1 = [d_0/d_1]^2 I_0 \quad (2)$$

In the experiment, the radiation source and the detector areactually separated by distance d_1 but we detect intensity $I \leq I_1$ because the radiation passes through material with density $\mu(x, y)$. So, we can write:

$$I = I_1 \exp\left[-\int_r \mu(x,y)dr\right] = [d_0/d_1]^2 I_0 \exp\left[-\int_r \mu(x,y)dr\right] \quad (3)$$

Isolating the integral of attenuation coefficients, we obtain:

$$\int_r \mu(x,y)dr = -\ln\left[\left(\frac{I}{I_0}\right)\left(\frac{d_1}{d_0}\right)^2\right] \quad (4)$$

The integral of attenuation coefficients along the ray path r can be calculate using this equation and the detected intensity I. The tomographic reconstruction determines the 2-D density distribution $\mu(x, y)$from many radiation intensities I in many paths r.

3.1.2. Reconstruction algorithms

Even before the appearance of commercial x-ray CT scanners for medical use around 1971, an old work from 1957 performed industrial gamma ray tomography using a fourth degree polynomial to represent the density distribution of matter [6]. A least squares algorithm calculated the polynomial coefficients that minimized the error between the polynomial and the irradiation data.

Modern reconstruction algorithms can be classified into three major groups. The first group includes analytical methods that apply a suitable linear operator, for example, the well-known filtered back projection(FBP) [18]. The second group comprises iterative algorithms such as Algebraic Reconstruction Technique (ART) [19-21] and Multiplicative Algebraic Reconstruction Technique(MART). The third group consists of machine learning-based algorithms that are currently being actively developed [22-24].

FBP is used by many works on industrial gamma ray tomography [10]. It is computationally efficient butneedsmany of radiation measurementswith low noise to obtainaccurate reconstructed images [18,19]. In our application, the number of measurements is limited and the data is noisy due to the experimental conditions.So, this algorithm is not appropriate.

Many recent papers use machine learning, especially convolutional neural network, to improve the quality of reconstruction [23]. They can be used in two major stages of image reconstruction: (1) after the reconstruction as a post-processing to attenuate noise or artifacts [22]; or (2) during the reconstruction, to help the system converge to the best solution [24]. We cannot apply this approach to our problem because a machine learning-based reconstruction algorithm usually requires large amount of high-quality data for training.

So, the iterative algorithms are the best choice for our problem. Iterative reconstruction algorithms typicallytake longer than FBP but they can produce good reconstructions even using few and noisy data, non-circular geometry, non-uniform distribution of source and detector of gamma radiation and some missing data. Moreover, it does not require large quantity of high-quality data for training, as machine learning-based algorithms.

3.1.3. The algorithm used in this work

We use Algebraic Reconstruction Technique (ART), an iterative solver of the system:

$$\boldsymbol{Ax=b} \qquad (5)$$

Vector $\boldsymbol{x}$ is the reconstructed image in vectorial form, that is, each element x_j is the estimated attenuation coefficient at pixel j. The i-th detected irradiation count is the element b_i of vector $\boldsymbol{b}$. The matrix $\boldsymbol{A}$ is the geometric arrangement of the gamma ray paths in the image. Each row $\boldsymbol{a}_i$ of the matrix $\boldsymbol{A}$ is the path of the i-th gamma ray and each column $\boldsymbol{a}_j$ of $\boldsymbol{A}$ is the pixel j of the image such that:

$$a_{ij} = \begin{cases} 1, & \text{if ray } i \text{ passes through pixel } j. \\ 0, & \text{otherwise} \end{cases} \qquad (6)$$

We use simple binary matrix to represent the irradiation geometry instead of ray/pixel intersection area model, because our reconstructed images are quite large (744x168 and 503x168 pixels) and we consider each ray to be a long and narrow rectangle 17 pixels wide and at least 168 pixels long. Consequently, it makes little difference between using binary matrix or intersection areasto model the irradiation geometry. If the rays were rectangles or triangles with only 1 or 2 pixels wide, it would be mandatory to use the ray/pixel intersection model.

ART uses the following equation to find an approximate solution of the system (5):

$$\boldsymbol{x}^{k+1} = \boldsymbol{x}^{k} + \lambda_k \frac{b_i - \langle \boldsymbol{a}_i, \boldsymbol{x}^k \rangle}{\|\boldsymbol{a}_i\|^2} (a_i)^t \qquad (7)$$

where $i$is an index (in our implementation, it follows a shuffled sequence), $||\boldsymbol{a}_i||^2$ is the quantity of pixels that ray i passes through (number of 1's in row$\boldsymbol{a}_i$) and λ_k is a relaxation parameter that decreases as the iteration step k increases.

In our application, often the density distribution of the equipment under analysis is known. This density distribution known a priori can be obtained in two ways: (a) from the design of the equipment and comprising the operation of the process; or (b) measuring the density distribution with the equipment off or on under ideal operating conditions. Therefore, if a priori distribution is known, the problem to be solved is to verifywhether the measured irradiation data agree (or not) with the expected density distribution[25, 26]. If they don't agree, we must determine where and how the two differ.ART can incorporate this knowledge settingx^0 with the prior density distribution. It is modified in successive iterations to conform to the obtained projection data.

When no prior knowledge is available, the initial density $x^0$is usually set to the mean density computed from the projection data.

3.1.4. Compressive sensing

Tomographic reconstruction usually does not have a single solution, because the system of equations (5) is usually highly under-determined.There are many more unknown variables than equations. So, we use compressive sensing (or compressed sensing). It chooses, among the images $\mu(x,y)$that satisfy the experimental data, the image that has minimal total variation (TV), i.e., the minimal absolute sum (l_1-norm) of gradient magnitude:

$$\min_{\mu(x,y)} \left\| g_{\mu(x,y)} \right\|_1 \quad \text{subject to } \boldsymbol{Ax} = \boldsymbol{b} \qquad (8)$$

where $g_{\mu(x,y)}$ is the gradient magnitude of the density distribution$\mu(x,y)$. Compressive sensing reconstruction algorithms usually intercalate total variation minimization filter between the iterations of the reconstruction algorithm [19,27] and we do the same.We implemented the algorithm proposed by Chambolle [28] in C++ and use it with parameters τ=0.225 and λ=0.015.

3.2. Collimation

Collimation is the process of emitting/collecting gamma rays only to/from a given direction. Traditionally, gamma ray collimation uses materials with a high atomic number Z such as lead or tungsten to attenuate divergent radiation, and is called hard, physical or mechanical collimation.

Although traditional gamma scanners have some wide-angle hard collimation at the sourcein order to increase radioactive safety, usually do not have mechanical collimation at the detector. If there was collimation in the detector, it would be very difficult to point the detector precisely in the direction of the source. The goal of classical gamma scan is to obtain the relative density profile of the inspected object by reading a large spectrum of transmitted photons (generally everything above 400 keV) and thus collimation in the detector is not necessary.

On the other hand, industrial gamma tomography for small objects generally uses a well-defined geometry with a mechanical device that automatically moves gamma ray source and detectors (or moves the scanned object with fixed source and detectors). In this case, hard collimated detectors can easily be adjusted to point at the gamma source and this ensures that only rays coming from the source direction are counted, allowing for sharper reconstructions.

In our preliminary laboratory 2-D gamma scan experiments, we used a mechanical device (gantry) that automatically aligned the radiation source and detector [12]. This allowed us to use hard collimation.

However, in industrial 2-D scan for demister evaluation, it is impossible to use hard collimation, because there is no way to make the source and detector point at each other. Moreover, hard collimation would make the collimated devices heavy, making difficult their use in the field. If we do not collimate, we would obtain a blurred reconstruction, because we would detect scattered radiation that originate from a wide angle.

We describe below a system that we call “electronic collimation for gamma scan”, which does not require heavy collimation apparatus or precise alignment of the source and the detector. Electronic collimation is a term usually associated with gamma cameras for determining the direction of the incoming gamma ray, using the Compton effect [31,32]. On the other hand, the electronic collimation for gamma scan is used to count only the gamma rays that pass through a narrow region between the source and the detector, also employingthe Compton effect.

3.2.1. Electronic collimation for gamma scan

Industrial process equipment is generally made of metal to mechanically withstand temperatures, pressures, environmental and process conditions. To inspect such equipment with the aid of gamma scan or tomography, medium to high energy gamma sources (such as Cs-137 - 0.662 MeV or Na-24 - 2.7 MeV) must be used. These photons are able to pass through the thick walls of the vessels and obtain information about the internal conditions. In this energy range, photons interact with matter through Compton scattering [29] and the resulting scattered photon has less energy that the incident photon (Figure 6).

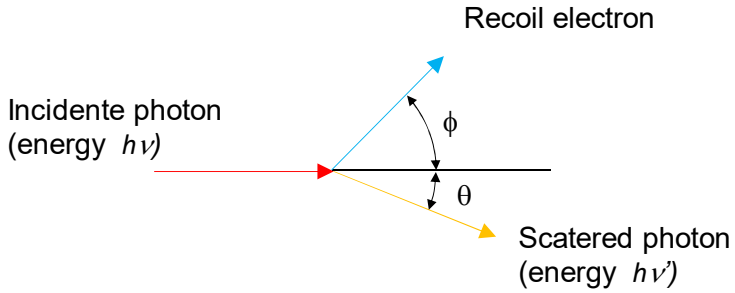

Figure 6. Compton scattering.

The formula and graph of the scattered photon energy for Cs-137 and Co-60 are presented in Figure 7 as a function of the scattered angle θ. This graph indicates that, if we take into account, for example, only photons with energy greater than 1.08 MeV, we will be counting only photons whose scattering angle is smaller than 25 and 16 degrees, respectively for Co-60 γ1 and γ2.

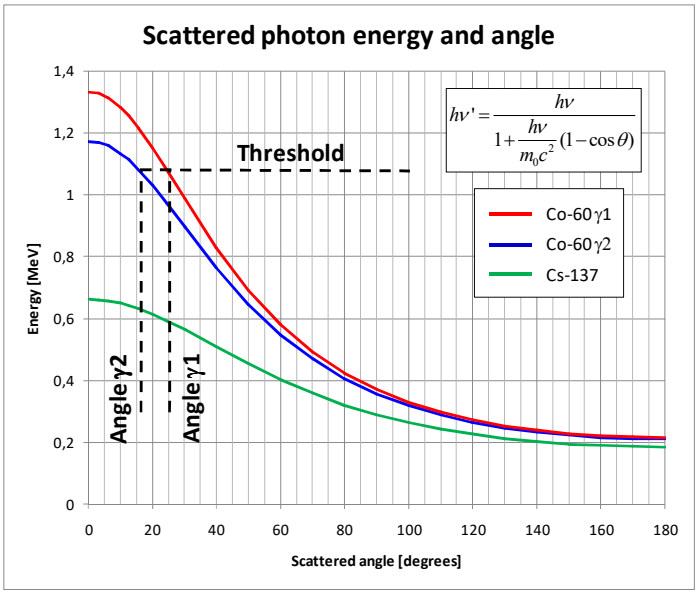

Figure 7. Energy of the scattered photon as a function of the scattering angle for Co-60 and Cs-137.Incident and scattered photon energies are denoted respectively as hν andhν', and $m_0c^2$is the mass energy of electron at rest.

An interesting consequence of this property is shown in Figure 8. Consider a source and detector of gamma radiation positioned at a distance many times greater than their sizes. If we count only the photons above a certain level of energy, we will measure only the photons that are scattered up to a certain angle. The maximum scattering angle will define an almond-shaped region located between the source and the detector. Photons with energy above the threshold may only have originated from this region. Photons with energy above the threshold can be detected without using any hard collimation device and without the need to mechanically point the detector and source at each other.

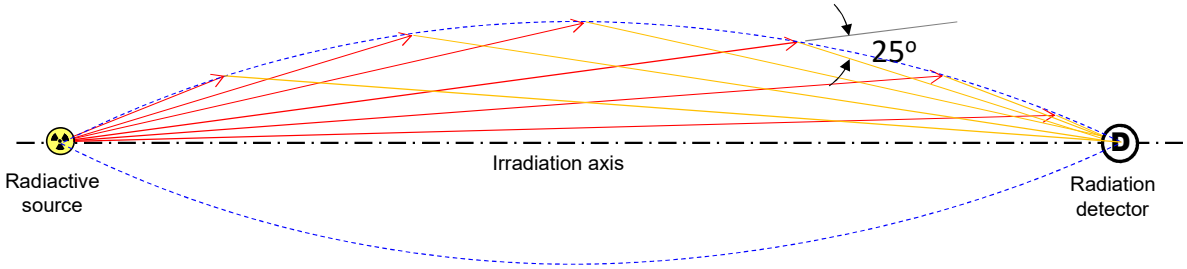

Figure 8. Spatial region defined by a limited scattered angle.

In conclusion, electronic collimation for gamma scan associates energy level of photon with a geometric region. The higher the energy threshold, the narrower the gamma ray beam. This technique allows obtaining tomographic data using non-collimated source and detector, without the aid of any mechanical device to align them [30]. In this work, we collected the data with a 1.080 MeV threshold, resulting in maximum angles of 16 and 25 degrees for the two gamma photons from the Co-60 source.

4. Evaluation of Demisters Using 2-D Gamma Scanning

This Section describes the tomographic 2-D gamma scan of a real industrial equipment. A large petrochemical plant in southwestern Brazil wanted to investigate if there is any problem in a dilution steam drum with three demisters, as a preparation for an incoming general maintenance shutdown. Neither the conventional gamma scan nor the industrial CT was able to adequately solve this problem. The conventional gamma scan would generate a 1-D plot that does not clearly point out the defect of the equipment. Industrial CT requires a circular geometry with parallel or fan-beam projections, which is obviously not the case.

In previous works, industrial tomographic 2-D scan had been applied only to process equipment with vertical orientation, where the source and the detector of gamma-ray could be positioned and moved in the vertical direction with the aid of gravity. In this horizontal-oriented equipment, the crew could not count on gravity to move the instruments. Manual movement and positioning of instruments was the simplest, fastest and most economical way to inspect this drum. This strategy was feasible due to the low activity of the source, good performance of the scintillation detectors, experience of the crew and good working strategy, resulting in a radiation dose undetectable by the dosimeter. The radiation dose received by each member in the month in which this project was carried out could not be detected by the dosimetric system, as it is below the minimum recordable value of 0.20 mSv. We were able to collect less than the ideal amount of data. Even so, the technique allowed to draw conclusions about the scanned equipment.

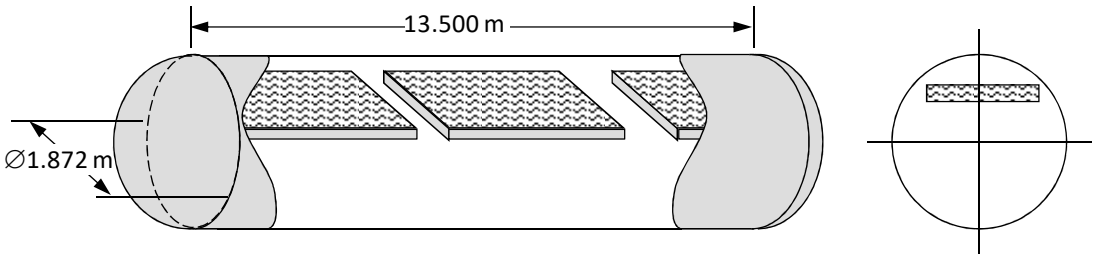

Figure 9. General arrangement of the vessel.

4.1. Procedures

To access the inspection region, two large scaffoldings were built. The vessel has many inlet and outlet pipes close to the imaging plane that prevent placing the source and detector of gamma rays in these positions. Due to access difficulties the scans were divided into two imaging areas, one covering the two leftmost demisters and the other covering the remaining right demister, as shown in Figure 10.

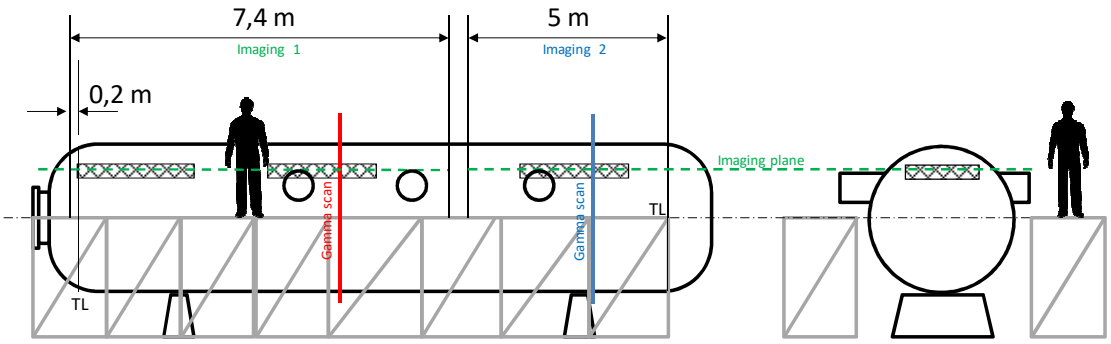

Figure 10. Layout of scaffoldings, positions of the conventional gamma scans (red and blue lines) and the imaging plane of tomographic 2-D gamma scan (dashed green line).

Two conventional gamma scans were performed at the middle and right demisters (Figure 10, red and blue lines) and the results indicated the approximate elevation of the demisters and the liquid level (Figure 11). After proper interpretation, these results allowed us to choose where the imaging plane should be located.

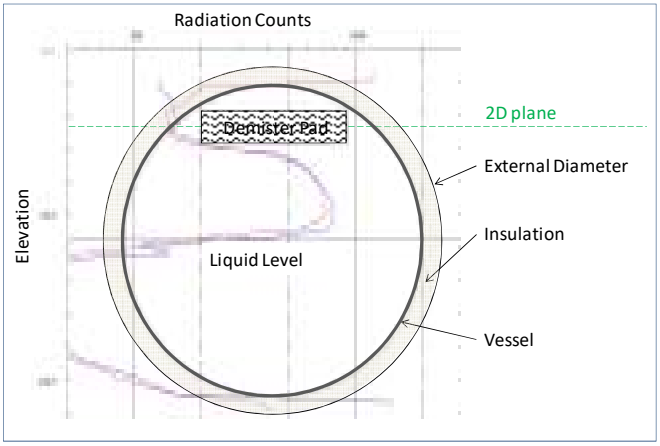

Figure 11. Regular gamma scans applied to two sections of the vessel. Red and blue graphs represent respectively densities at central and right demisters.

After determining the imaging plane, we defined all positions of the source and detector of gamma ray with a 20 cm spacing and a maximum inclination of ±45 degrees (Figure 12). The positions where it was impossible to place the source or detector of gamma ray (due to the presence of rings, supports, nozzles, etc.) were excluded, that is, no equipment was be positioned in those coordinates. For data acquisition, we used a standard non-collimated source and detector, with only a small hardware change: we placed equipment holders that allowed us to manipulate and position them.

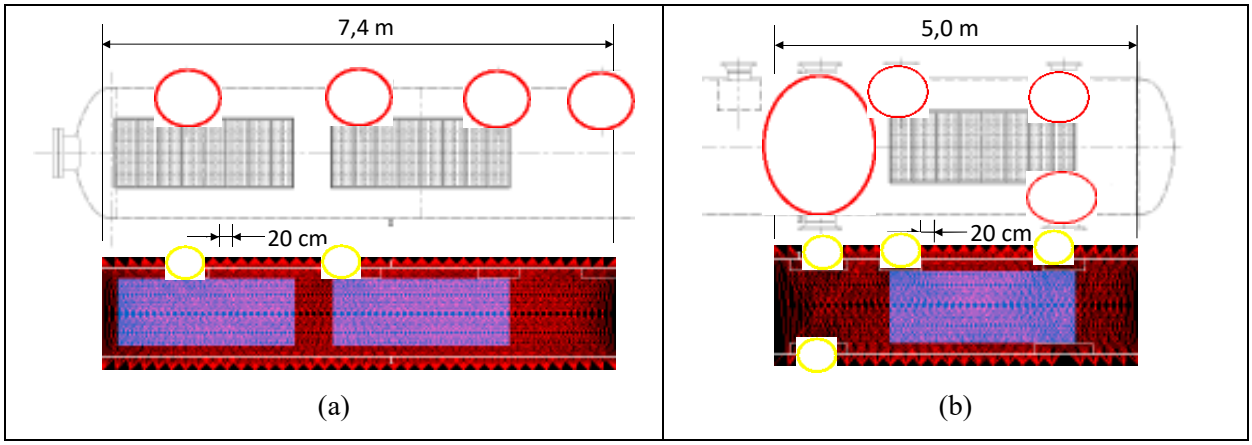

Figure 12. Sketch of the equipment with gamma ray paths (red lines) and positions of gamma ray source and detector. Red ellipses highlight the internal structures that generate false regions of high density in the reconstructions. Yellow ellipses highlight the regions without irradiation data that introduced errors in the reconstructions.

Each demister pad consists of 8 rectangular modules mounted side-by-side on a supporting frame welded inside of the drum. Figure 13 depicts a typical aspect of twomodules similar to those installed on the vessel. We used a 8.1 mCi Co-60 radioactive source coupled with a 2 inch NaI(Tl) scintillation detector in all conventional and 2-D gamma scans.

Figure 13. Two steam drum demisters similar to those installed in the inspected equipment. Courtesy of BeggCouslandEnvirotec Limited.

We collected 544 and 282 gamma ray counts to perform the two tomographic 2-D gamma scans. We show in Figure 14 how we organized these data as text files. The first two lines say that we get 277,500 radiation counts when gamma ray source and detector are spaced 167 cm in vacuum or air (respectively I_0 and d_0 in equation 4). Each gamma ray irradiation data was written as 5 numbers: (x_src, y_src) (x_det, y_det) radiation_count, where the distance between the source and the detector is d_1 and radiation_count is I in equation 4. If we plot only the transverse data, we obtain the 1-D graph that would be obtained in a conventional 1-D scan (Figure 15).

Vacuum_radiation_count=277500	Vacuum_radiation_count=277500
Vacuum_distance_in_cm=167	Vacuum_distance_in_cm=167
Number_of_counts=544	Number_of_counts=282
(0, 0) (0, 167) 11123	(0, 0)(0, 167) 10014
(0, 0) (20, 167) 7543	(0, 0)(20, 167) 10655
...	...

Figure 14. The beginnings of the two text files with the gamma scan data. An irradiation data is denoted by five numbers:(x_src, y_src) (x_det, y_det) radiation_count.

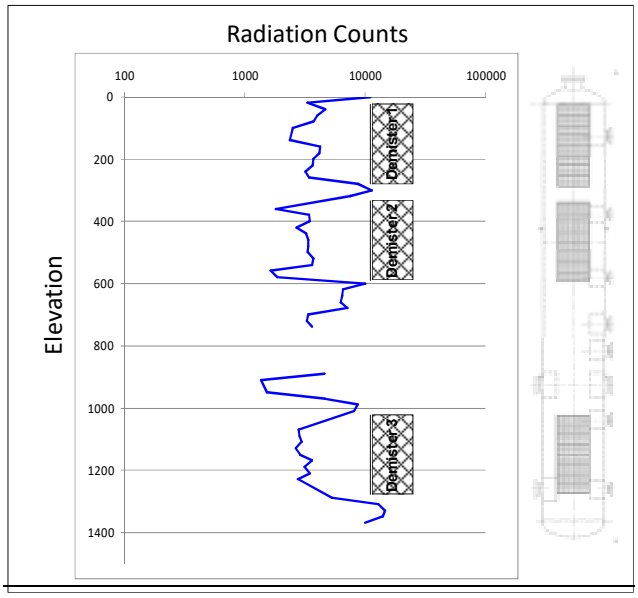

Figure 15. A simple 1-D scan plot can be obtained from the tomographic 2-D gamma scan data.

We implemented ART reconstruction algorithm with total variation minimization in C++. The domains of the reconstructed images were 744x168 pixels (the two leftmost demisters) and 503x168 pixels (the right demister). Each gamma ray irradiation was represented as a long and narrow rectangle 17 pixels wide, starting at the coordinate (x_src, y_src) and ending at the coordinate (x_det, y_det). We experimentally chose the width of 17 pixels and will use this value throughout this paper. The row i of matrix $\boldsymbol{A}$ (equation 5) represents the i-th rectangle (gamma ray) and the column j of matrix $\boldsymbol{A}$ represents the image pixel j. If pixel j belongs to the rectangle i, then a_{ij}=1, and a_{ij}=0 otherwise. We do not actually store matrix $\boldsymbol{A}$ in computer because it is huge, with MxN elements, where M is the number of pixels of the image and N is the number of irradiations. We store only the image x^k, that is much smaller (with only M elements). We compute the elements of matrix $\boldsymbol{A}$ only when necessary.

4.2. Results

Figure 16a shows the color scale that we use throughout this paper to represent the density profiles generated by the reconstruction algorithm. Figure 16b shows the color scale that we use to represent a priori density distribution. Figure 17a depicts the sketch of the equipment and Figures 17b-e depict the first reconstructed images we obtained, without using any a priori density distribution. In this case, we initialized x^0 in equation (7) with a constant value, the average density computed from the irradiation data. The obtained results are disappointing, because no demister is visible. Looking at these images, it is not possible to know if the demisters are in their right places. Worse still, the reconstructed images change according to the parameters used in the ART reconstruction. Figures 17b-c depict the images reconstructed with 3 ART iterations with λ = (0.5, 0.25, 0.125) in equation (7). Figures 17d-e depict the images reconstructed with 63 ART iterations with λ starting at 0.5 and decreasing by factor of 0.95. The two reconstructions are considerably different.

As we said before, tomographic reconstruction is a highly under-determined problem. The reconstructed images in Figures 17b and d have 744x168=124,992 pixels (unknown variables) but only 544 equations (radiation counts), while the reconstructed images in Figures 17c and e have 503x168=84,504 unknown variables and only 282 equations. So, there are many different images that satisfy the collected data. Furthermore, the equipment's steel walls are much denser

(≈0.42/cm) than the demisters (≈0.01/cm) and we have no horizontal irradiation, what makes it impossible for the reconstruction algorithm find out by itself where the high-density horizontal walls are located.

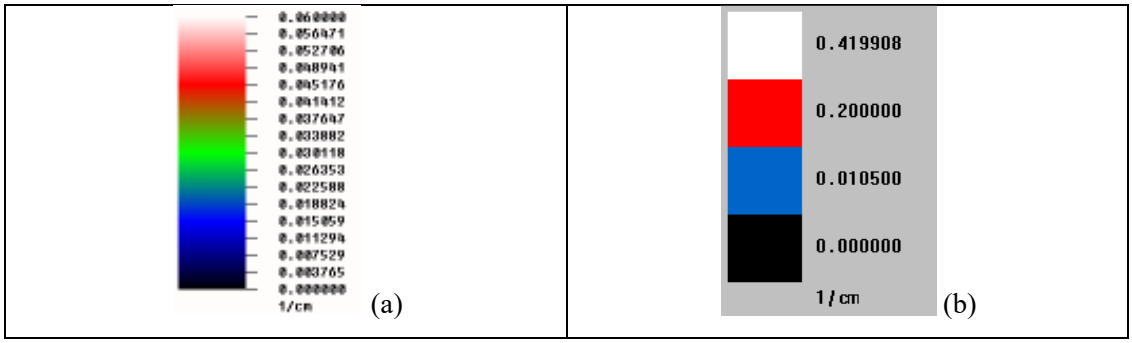

Figure 16. Color scales of density used throughout this paper. (a) Scale used to represent density profiles generated by the reconstruction algorithm. Any material denser than 0.06 is represented as white. (b) Scale used to specify a priori density distribution (white=steel, red=thin steel wall, blue=demister, black=air).

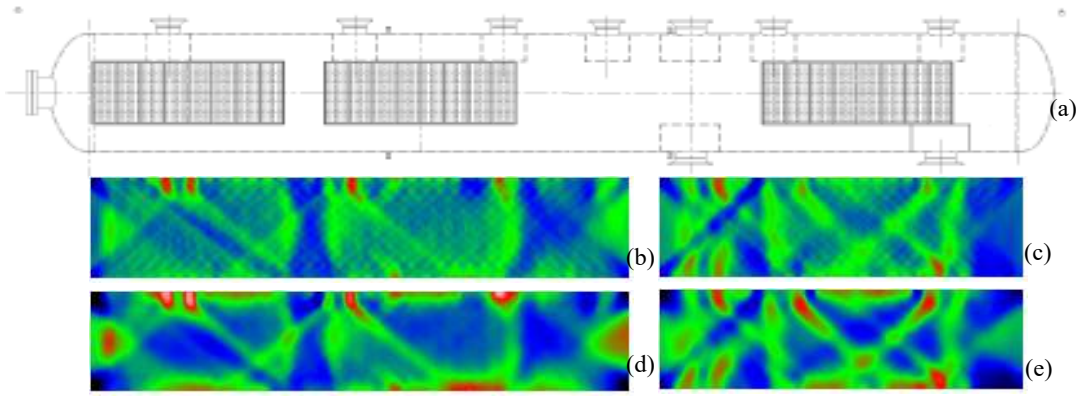

Figure 17. (a) The sketch of the equipment. (b-e) The images reconstructed without using prior density distribution.(b-c) With 3 iterations of ART algorithm. (d-e)With 63 iterations.

Fortunately, we know from the construction plans of the equipment where the steel walls are, as well as their approximate thickness and density. We also know where demisters should be located if they have not been damaged as well as their approximate density. We can use this prior knowledge as the starting point (x^0 in equation 7) of the ART reconstruction algorithm. Figures 18a-b depict prior density distribution we used with the steel walls of the vessel and the three demisters inside steel boxes. Figures 18c-d depict the obtained reconstruction using this prior knowledge, where the three demisters can be seen faintly. Note that the total variation filter managed to keep the steel walls sharp in the reconstructed images, not spreading their high density over the image. 2-D gamma scan has no longitudinal (horizontal) irradiations and therefore cannot locate the walls of the equipment. Using a priori information, it was possible to reconstruct the walls even without longitudinal irradiations. The number of iterations of our algorithm is not critical, because it can vary within a certain range without major changes in the reconstructed image. We obtain visually similar reconstructions using 3, 5 or 8 iterations. In this and following reconstructions we iterated ART 5 times with λ = (0.5, 0.35, 0.245, 0.1715, 0.1200).

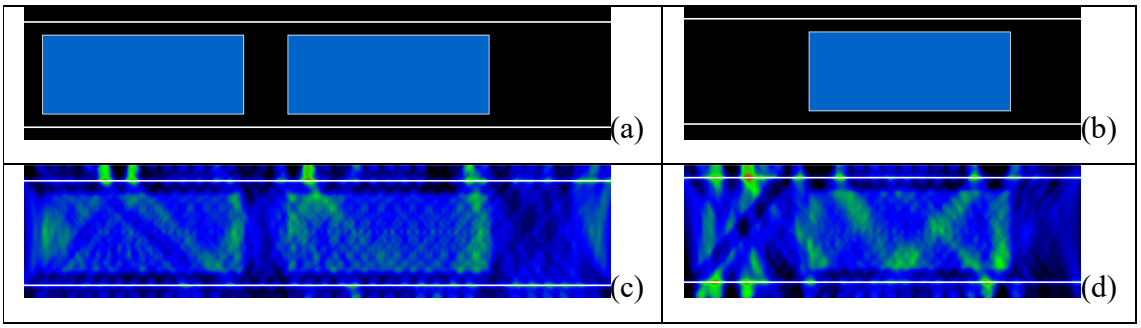

Figure 18. (a-b) A priori known density distribution. (c-d) The obtained reconstruction of the demisters using prior density.

Is there any other prior knowledge that we can use to further improve the quality of reconstruction? We are sure that, outside the vessel, there is only air with density close to zero. Actually, there are parts like rings, supports, nozzles, etc., but they can be ignored because we do not want to make them visible in the reconstruction and we put the source and detector of gamma ray so that the ray paths do not cross these external structures. Thus, we entered two artificial

irradiation data (Figure 19), one on the left side and the other on the right side of the equipment (below and above the vessel walls in Figure 20), with the radiation count we would obtain in the air. These counts that can be calculated using equation (2).

(0, 10) (740, 10) 14132	(0, 10) (500, 10) 30957
(0, 158) (740, 158) 14132	(0, 158) (500, 158) 30957

Figure 19. Artificial data we used to inform the algorithm that there is only air outside the vessel, where the five numbers mean (x_src, y_src) (x_det, y_det) radiation_count.

Using these two artificial data, we obtained the reconstructed images depicted in Figure 20. The reconstructed image is now almost entirely black outside the vessel, due to the artificial data, and the demisters can be seen more clearly. When we look at the reconstructed images (Figure 20) together with sketch of the equipment and gamma ray paths (Figure 12), we can conclude that the small structures (nozzles, baffles, supports, etc.) are the source of most of the "defects" we observe in the reconstructed images. The internal structures introduce false dense regions, because the gamma ray passes through them but the reconstruction algorithm is unable to reconstruct them (red ellipses in Figures 12 and 20c-d). The external structures prevent instruments from being positioned and thus create regions without irradiation datarepresented as stripes with high or low density (yellow ellipses in Figures12 and 20c-d).

The industrial tomographic 2-D gamma scanning indicated that there is no evidence of missing demister pad in the scanned equipment.

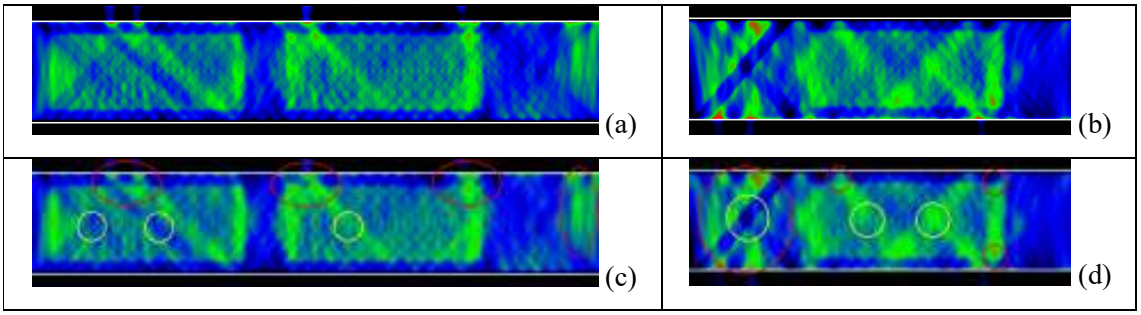

Figure 20. (a-b) Images reconstructed using the two artificial irradiation data outside the vessel. (c-d) The same images with ellipses highlighting regions with probably false density.

5. Simulations and Qualitative Evaluations

We did simulations to certify that, if there were any mechanical defects in the demisters, we would see them in the reconstructed images. In this project, the customer was not concerned about fouling because it is very difficult to happen due to the operating conditions. Consequently, we did not simulate scenarios with fouling. The simulations also allowed us to assess quantitatively and qualitatively the superiority of the 2-D gamma scan over the conventional 1-D method.

Collecting and analyzing data, we realized that the initial a priori density distribution (shown in Figure 18a-b) was slightly wrong. We noticed that the demisters are probably a little denser than we anticipated, and so we corrected their density from 0.0105 cm^{-1} to 0.017cm^{-1} (from now on, blue represents 0.017 cm^{-1} in prior density). We also realized that the steel boxes containing the demisters are probably a little thinner than we initially thought. As these boxes are represented with one pixel thickness, there is no way to make them even thinner in the images. Thus, we decreased their densities from 0.42 cm^{-1} to 0.2 cm^{-1} (represented by red in prior density).

5.1. Equipment without defect

We first generated the expected density distribution supposing that all demisters are in their correct places, without any internal high-density parts to hinder reconstruction (Figures 21a-b). Using the same irradiation geometry we used in the real experiment (Figure 12), we artificially calculated the 546+284 radiation counts from the expected density. We made reconstructions from this simulated data using Figures 21a-b themselves as prior density distributions, with the same parameters used in real reconstruction, obtaining the reconstructed images in Figures 21c-d. All demisters are clearly visible and almost noiseless in the reconstructed images.

The conventional 1-D gamma scan uses only transverse (vertical) irradiations to plot a 1-D graph. Thus, the maximum information that can be obtained from a conventional 1-D gamma scan is the column by column average density (Figures 21 e-f). The quality of a real 1-D gamma scan would be much worse than this ideal simulation: it would have far less irradiation data, the edges would be blurred, etc. Even in this ideal condition, the errors made by the 1-D gamma scan are approximately 3 times larger than those made by the 2-D gamma scan (Table 1). Even if we

subtract the density of the steel walls (Figures 21 g-h), the errors of the 1-D scan are still much larger than 2-D.

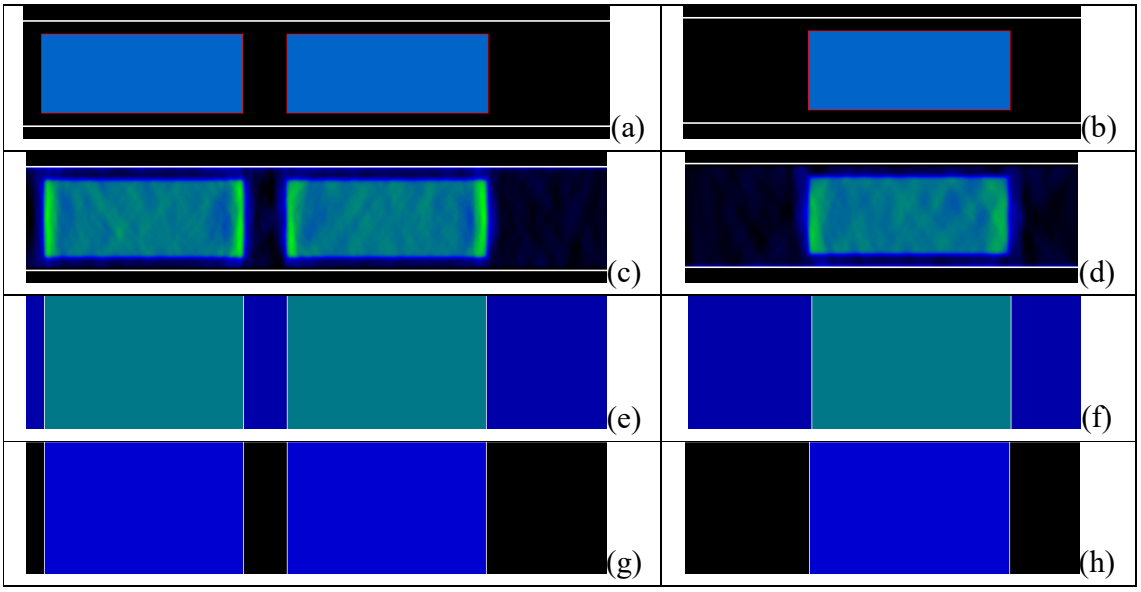

Figure 21. Simulations of 2-D and 1-D gamma scans from density distributions where all demisters are in the correct places. (a-b) Simulated densities. (c-d) 2-D reconstructions. (e-f) Ideal1-D scans obtained calculating column by column means. (g-h) Ideal1-D scansobtained subtracting the density of steel walls.

Table 1. Errors made by2-D reconstructionsand ideal 1-D scans in Figure 21.

Differencebetween 21a and	MAE (cm^{-1})	RMSE (cm^{-1})	Differencebetween 21b and	MAE (cm^{-1})	RMSE (cm^{-1})
21c	0.0073	0.0221	21d	0.0061	0.0197
21e	0.0224	0.0656	21f	0.0217	0.0652
21g	0.0169	0.0664	21h	0.0163	0.0665

5.2. Large defects

Then, we simulated what we would observe if largechunks of demisterswere missing, without any internal high-density parts (Figure 22). We used as prior density the images with all demisters in their places (Figures 21a-b). The tomographic scan clearly identifies the missing chunks. In this case, it is possible to diagnose the defects even using 1-D scan. Again, the 2-D scan errors are substantially smaller than those of 1-D scans (Table 2).

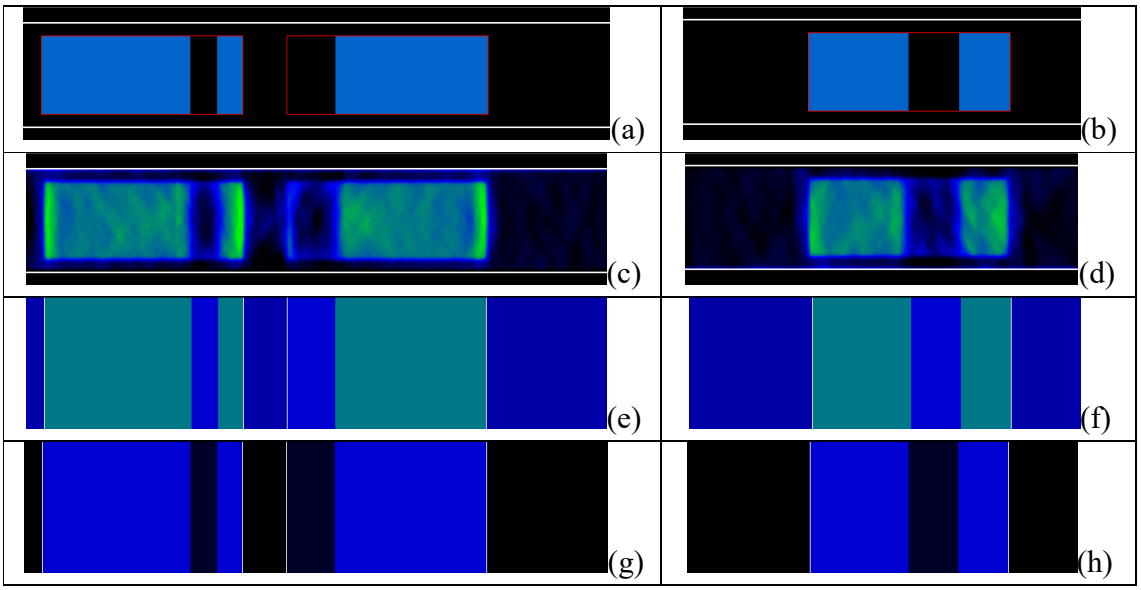

Figure 22. Simulations of 2-D and 1-D gamma scans from density distributions with large missing chunks of demisters. (a-b) Simulated densities. (c-d) 2-D reconstructions. (e-f) Ideal 1-D scans obtained calculating column by column means. (g-h) Ideal 1-D scans obtained subtracting the density of steel walls.

Table 2. Errors made by 2-D reconstructions and ideal 1-D scans in Figure 22.

Difference between 22a and	MAE (cm^{-1})	RMSE (cm^{-1})	Difference between 22b and	MAE (cm^{-1})	RMSE (cm^{-1})
22c	0.0075	0.0224	22d	0.0063	0.0201
22e	0.0225	0.0658	22f	0.0218	0.0654
22g	0.0163	0.0665	22h	0.0145	0.0661

5.3. Small defects with internal parts

Finally, we simulated what we would observe if small parts of demisters were missing and if there were some internal high-density parts, as uses to happen in real equipment. As before, we generated the simulated density distributions (Figures 23a-b). Using the same irradiation geometry we used in the real experiment (Figure 12), we computed artificially the 546+284 radiation counts. We made reconstructions from the simulated data using as prior density Figures 21a-b without defects or internal parts. We obtained the reconstructed images (Figures 23c-d), where it is possible to visualize (albeit with distortions) the missing pieces of demisters and internal high-density structures.

Figures 23e-f depict the column by column average, the maximum information that can be obtained using the conventional 1-D gamma scan. Looking at them, it is not possible to guess what is wrong with the demisters.

The errors obtained are depicted in Table 3. Again, the 1-D scan errors are far greater than 2-D errors. Even if we subtract the density of the steel walls (Figures 23g-h), 1-D scan errors remain much larger than the 2-D scan errors.

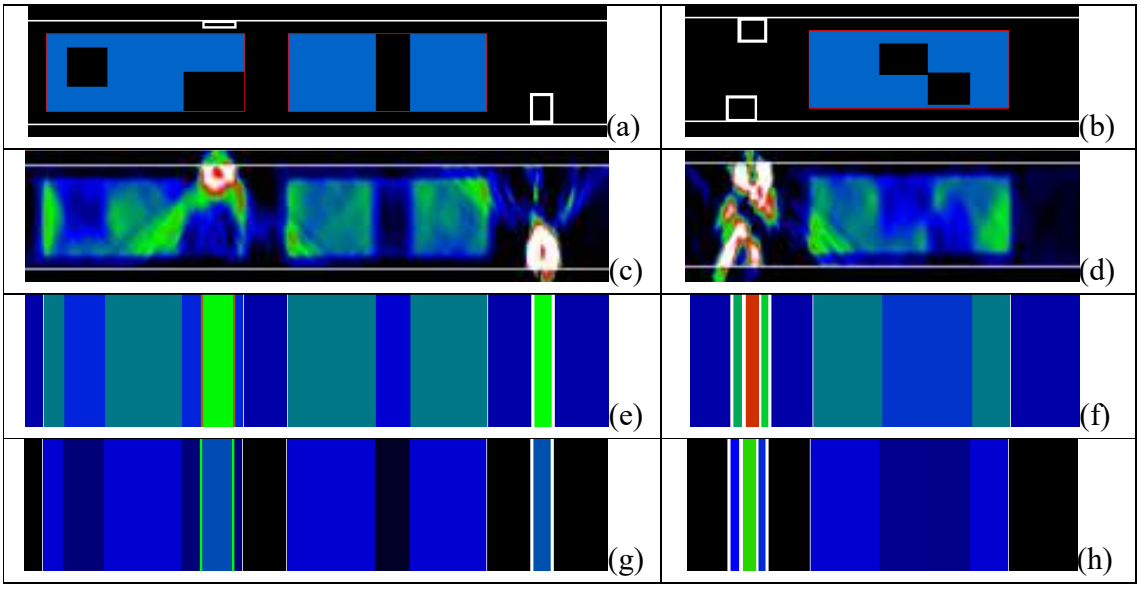

Figure 23. Simulations of 2-D and 1-D gamma scans from density distributions with small pieces of demisters missing and internal high-density parts. (a-b) Simulated densities. (c-d) 2-D reconstructions. (e-f) Ideal 1-D scans obtained calculating column by column means. (g-h) Ideal 1-D scans obtained subtracting the density of steel walls.

Table 3. Errors made by 2-D reconstructions and ideal 1-D scans in Figure 23.

Differencebetween 23a and	MAE (cm^{-1})	RMSE (cm^{-1})	Differencebetween 23b and	MAE (cm^{-1})	RMSE (cm^{-1})
23c	0.0118	0.0361	23d	0.0137	0.0441
23e	0.0266	0.0720	23f	0.0289	0.0761
23g	0.0205	0.0727	23h	0.0227	0.0767

5.4. Qualitative evaluation of 1-D and 2-D scans

The conventional 1-D scan and the 2-D tomographic scan are so different technologies that it is difficult to make a direct comparison. We converted 1-D graphs to 2-D images to make numerical comparison, but it is unclear whether the errors obtained accurately reflect the amount of information. We make the following qualitative considerations between 1-D and 2-D scan.

First of all, usually a conventional 1-D gamma scan is a cross section scan, as shown in Figure 11. Evidently, in this case, the scan would identify the missing demister only if the scan is performed in the exact missing demister plane.

Even if a horizontal gamma is performed, generating a density profile similar to that of Figure 15, the result would not accurately indicate the condition of the demisters. Looking at the graph in Figure 15, would the reader say without a doubt that there is no defect in any of the demisters? Even when we look at the graph together with the equipment sketch (Figure 15 on the right) it is not clear whether any dense parts are masking some missing piece of demister. Meanwhile, looking at Figures 20a-b together with the equipment sketch in Figure 17a, it is clear that no demister is missing. In addition, all the high-density internal structures are represented in the reconstructed images, although not clearly.

Let us look at the idealized simulations of Figures 21 and 22. In these ideal scenarios, there are no internal high-density parts and, when there are defects in the demisters, large chunks are missing. In these cases, both 2-D and 1-D scans can diagnose the defects.

Figure 23 shows small defects with some internal high-density parts. In Figure 23g (1-D scan), it is very difficult to diagnose the missing demister because the internal parts interfere with the density profile. Meanwhile, in Figure 23c (2-D scan), all the missing pieces of demisters are visible, even with the interference of the high-density structures. Similarly, in Figure 23h (1-D scan), it is impossible to spatially localize the missing demisters. Meanwhile, in Figure 23d (2-D scan) the missing parts can be easily located.

6. Conclusions

In this paper, we described the application of industrial tomographic 2-D gamma scanning to a long horizontal vessel with three demister pads to evaluate possible mechanical problems. Moving instruments only parallel to the vessel axis, the 2-D scan was able to reconstruct the rectangular image of the density of the equipment interior. It is very difficult to mechanically collimate the gamma detector in the field, because it is almost impossible to point the detector precisely at the gamma source. On the other hand, the collimation is necessary to obtain clear reconstructions. We presented a technique we called “electronic collimation for gamma scanning” that is able to count only the rays that pass through a narrow region between emitter and detector, even without mechanical collimation. The dilution steam drum posed several new challenges to perform industrial 2-D gamma scan. In this equipment, there are many external and internal structures at the height of the scanning plan that difficults the reconstruction. External structures hinder free positioning of the instruments and internal structures create false dense regions. Moreover, demisters are about 40 times less dense than steel and 6 times less dense than water, what makes it difficult for the algorithm to reconstruct them clearly. Most importantly, 2-D scan does not have longitudinal (horizontal) irradiations that allows the equipment walls to be correctly located. We overcame these difficulties by using approximate density distribution of the equipment known a priori, together with artificial irradiation data. We also ran simulations to show the superiority of 2-D gamma scan over conventional 1-D scan. These simulations also showed that, if there were defects in the demisters, we would observe them in the reconstructed images.

AUTHOR INFORMATION

Corresponding Author

Dr. Marcio I. Haraguchi.

TechnicalDirector, Tricom Tecnologia e Serviços de Manutenção Industrial, Ltda.

Rua Bartolomeu de Ribeira, 93, São Paulo, SP, Brazil, 05331-030.

marcio@tricomtecnologia.com.br

REFERENCES

[1] H.Z. Kister, Distillation Operation, McGraw-Hill,ed. 1, pp. 425-430, 1990.

[2] N.F. Urbanski, M.R. Resetarits, M.S.M. Shakur, Gamma scanning a column containing closely spaced trays, Annual Meeting AIChE 1999 - Separations Topical Conference, Dallas, TX, 1999.

[3]K. Laraki, R. Alami, R.C. El Moursli, A. Bensitel, L. El Badri, An expert system for improving the gamma-ray scanning technique, Nuclear Instruments and Methods in Physics Research Section A: Accelerators, Spectrometers, Detectors and Associated Equipment, 578(1) (2007) 340-344.

[4]H. Shahabinejad, S. A. H. Feghhi, M. Khorsandi, Impact of measurement approach on the quality of gamma scanning density profile in a tray type lab-scale column, Radiation measurements 61 (2014) 1-5.

[5]K. El Korchi, R. Alami, S. Mimount, A. Saadaoui, A. Chaouch,Coking phenomenon detection in liquid flow through a solid phase in a lab-scale distillation column using radioisotope techniques, Measurement, 110 (2017) 339-343.

[6] R.N. Bartholomew, R.M. Casagrande, Measuring solids concentration in fluidized systems by gamma-ray absorption, Industrial & Engineering Chemistry, 49.3 (1957) 428-431.

[7] G.A. Johansen, P. Jackson, Radioisotope Gauges for Industrial Process Measurements, John Wiley & Sons Ltd., pp. 240-245, 2004.

[8]L. De Chiffre, S. Carmignato, J.P. Kruth, R. Schmitt, A.Weckenmann,Industrial applications of computed tomography, CIRP annals, 63(2) (2014) 655-677.

[9]J. Kim, S. Jung, J. Moon, G. Cho, Industrial gamma-ray tomographic scan method for large scale industrial plants, Nuclear Instruments and Methods in Physics Research Section A: Accelerators, Spectrometers, Detectors and Associated Equipment, 640(1) (2011) 139-150.

[10] J. Kim, S. Jung, J. Kim, A study on industrial gamma ray CT with a single source-detector pair, Nuclear Engineering and Technology, 38(4) (2006) 383-390.

[11]Z. Kuzeljevic, M.Dudukovic, H. Stitt, From Laboratory to field tomography: data collection and performance assessment, Industrial & engineering chemistry research 50.17 (2011): 9890-9900.

[12] M.I. Haraguchi, H.Y. Kim, W.A.P. Calvo, Tomographic 2-D gamma scanning for industrial process troubleshooting, Flow Measurement and Instrumentation, vol. 62, pp. 235-245, 2018.

[13] A.S. Al-Dughaither, A.A. Ibrahim, W.A. Al-Masry, Investigating droplet separation efficiency in wire-mesh mist eliminators in bubble column, Journal of Saudi Chemical Society, vol. 14, pp. 331-339, 2010.

[14]S.X. Xu, G. Kennedy, C. Conforti, T. Marut and J. Dusseault, Troubleshooting Industrial Packed Columns by Gamma-Ray Tomography, CE Expo'99, p. 1, 1999.

[15]M. Khorsandi, S.A.H. Feghhi, Gamma-ray CT as a complementary technique for structural inspection of tray-type distillation columns, Measurement 78 (2016) 1-8.

[16]D. Saengchantr, S.Srisatit, N.Chankow, Development of gamma ray scanning coupled with computed tomographic technique to inspect a broken pipe structure inside laboratory scale vessel, Nuclear Engineering and Technology 51.3 (2019) 800-806.

[17] M.I. Haraguchi, H.Y. Kim, R.O. Machado, Tomografia Industrial Computadorizada, XXVIII Congresso Nacional de Ensaios Não Destrutivos e Inspeção, Santos, SP, 2009 (in Portuguese).

[18] X. Pan, E.Y. Sidky, M. Vannier, Why do commercial CT scanners still employ traditional, filtered back-projection for image reconstruction?, Inverse problems, 25(12) (2009) 123009.

[19] A. Biçer, Compressed sensing based computerized tomography imaging, Ph.D. Thesis, Middle East Technical University, 2012.

[20] R. Gordon, R. Bender, G.T. Herman, Algebraic reconstruction techniques (ART) for three-dimensional electron microscopy and x-ray photography, Journal of Theoretical Biology, 29(3) (1970) 471-481.

[21] G.T. Herman, A. Lent, Iterative reconstruction algorithms,Comput. Biol. Med., 6 (1976) 273-294.

[22]K.H. Jin, M.T. McCann, E. Froustey, M. Unser, Deep convolutional neural network for inverse problems in imaging,IEEE Tran. Image Processing, 26(9) (2017) 4509-4522.

[23]G. Wang, J.C. Ye, K. Mueller, J. A. Fessler, Image reconstruction is a new frontier of machine learning,IEEE Trans.Medical Imaging, 37(6) (2018) 1289-1296.

[24]H. Gupta, K.H. Jin, H.Q. Nguyen, M.T. McCann, M. Unser, CNN-based projected gradient descent for consistent CT image reconstruction,IEEE Trans.Medical Imaging, 37(6) (2018) 1440-1453.

[25]C.C. Gong, L. Zeng, C.X. Wang, Image reconstruction model for limited-angle CT based on prior image induced relative total variation, Applied Mathematical Modelling 74 (2019): 586-605.

[26]E.A. Rashed, H. Kudo, Statistical image reconstruction from limited projection data with intensity priors, Physics in Medicine & Biology 57.7 (2012) 2039.

[27]H. Yu and G. Wang, Compressed sensing based interior tomography, Phys. Med. Biol., 54 (2009) 2791-2805.

[28] A. Chambolle, An algorithm for total variation minimization and applications, Journal of Mathematical Imaging and Vision, 20.1-2 (2004) 89-97.

[29] G.F. Knoll, Radiation Detection and Measurement, 4th edition, John Willey & Sons (2010)50-52.

[30] M.I. Haraguchi, Imaging system for industrial equipment and process, 2018, patented, PCT/BR2018/050248

[31] N. Dogan, D.K. Wehe and A.Z. Akcasu, A source reconstruction method for multiple scatter Compton cameras, IEEE transactions on nuclear science 39.5 (1992): 1427-1430.

[32] J.E. Gormley, W.L. Rogers, N.H. Clinthorne, D.K. Wehe and G.F. Knoll, Experimental comparison of mechanical and electronic gamma-ray collimation, Nuclear Instruments and

Methods in Physics Research Section A: Accelerators, Spectrometers, Detectors and Associated Equipment 397.2-3 (1997): 440-447.

GraphicalAbstract